# Nanoscale

Accepted Manuscript


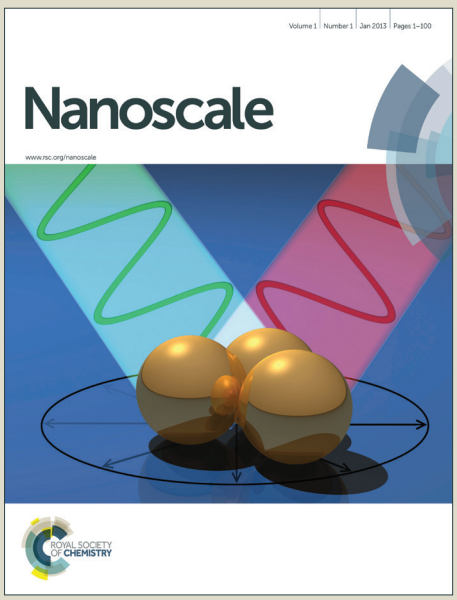





ROYAL SOCIETY OF CHEMISTRY

www.rsc.org/nanoscale

Cite this: DOI: 10.1039/c0xx00000x

www.rsc.org/xxxxxx

ARTICLE TYPE

# Facile fabrication of hierarchical $ZnCo_2O_4$/NiO core/shell nanowire arrays with improved lithium-ion battery performance

**Zhipeng Sun,[a,b] Wei Ai,[a] Jilei Liu,[a] Xiaoying Qi,[c] Yanlong Wang,[a] Jianhui Zhu,[a] Hua Zhang[c] and Ting Yu*[a, d, e]**

***Received (in XXX, XXX) Xth XXXXXXXXX 20XX, Accepted Xth XXXXXXXXX 20XX***
**DOI: 10.1039/b000000x**

We report a facile and controllable strategy for the fabrication of three-dimensional (3D) $ZnCo_2O_4$/NiO core/shell nanowire arrays (ZCO/NiO NWs) on nickel (Ni) foam substrate by a simple, cost-effective two-step solution-based method. Ultra-thin NiO nanosheets are revealed to grow uniformly on the porous $ZnCo_2O_4$ nanowires with many interparticle mesopores, resulting in the formation of 3D core/shell nanowire arrays with hierarchical architecture. In comparison with the pristine $ZnCo_2O_4$ nanowire arrays (ZCO NWs), the ZCO/NiO NWs exhibit significantly improved Li storage property in terms of higher capacity, enhanced rate capability and improved cycling stability when applied as the binder and additive-free anode materials for lithium-ion batteries (LIBs). The superior Li storage performance of the ZCO/NiO NWs could be attributed to the synergetic effect between the $ZnCo_2O_4$ core and NiO shell as well as its unique hierarchical architecture, which can ensure large specific surface area and good conductivity. Our achieved results may offer very useful guidelines in scrupulously designing 3D core/shell nanowire array electrodes by using cheap, earth-abundant materials for energy storage applications.

## Introduction

With an ever increasing list of promising applications, there is a surge in developing efficient and scalable strategies for fabricating nanostructures with diverse and tunable properties.[1-3] Recently, growth of heterostructures with controllable dimensions has sparked great research interest owning to the fact that diverse properties can be generated by tailoring the morphology, composition, and assembling organization of the primary nanobuilding blocks.[4-6] Most current research work has been focused on freestanding core/shell nanowire heterostructures due to their large surface areas, high surface/body ratios, more active surfaces sites, good ionic/electronic conductivities as well as better permeabilites in nanoscale electronics, catalysis, chemical sensing, and energy storage device applications.[7-15] Particularly, to serve as electrode materials for LIBs[10-12] and supercapacitors,[13-15] tremendous efforts toward freestanding core/shell nanowire heterostructures have been witnessed, from which heterostructured nanowire architecture can make use of the advantages of both components and offer special properties through a reinforcement or modification of each other.[13] For instance, a high performance of $SnO_2/V_2O_5$ core/shell nanowires as LIBs electrode have been obtained, which is owing to the synergetic effect exerted by $SnO_2$ and $V_2O_5$ as well as the unique core/shell structure.[16] Moreover, $Co_3O_4/TiO_2$ core/shell nanowires as LIBs anode also present high reversible capacity, improved cycling stability and excellent rate capability compared with the pristine $TiO_2$, which is in virtue of the synergistic effect of both the component and short diffusion length of the thin $Co_3O_4$ nanosheets.[17] Additionally, ordered $TiO_2/\alpha$-$Fe_2O_3$ core/shell nanowire arrays on carbon textiles as LIBs anode exhibit high rate capability and outstanding cycling performance as well.[11] Similarly, some core/shell nanowire or nanotube arrays such as $WO_{3-X}/MoO_{3-X}$,[15] $Co_3O_4/MnO_2$,[18] $NiCo_2O_4/MnO_2$[19] as electrode materials all exhibit enhanced capacitive performances and excellent stabilities for supercapacitors. For these above applications, it is extremely desirable to fabricate freestanding core/shell nanowire heterostructures due to their enhanced physical and chemical properties as compared to the single components.[20] Significantly, the interface/chemical distributions are homogeneous at the nanoscale and a fast ion and electron transfer is guaranteed.[10] Furthermore, it generally provides a high surface area to increase the interfacial kinetics, porous texture to accommodate the stress relaxation and a direct pathway for electron transport.[3,6]

To date, $ZnCo_2O_4$ and NiO have been considered as two kinds of anode materials with the superiority to graphite for lithium storage because of their high theoretical capacity, low cost, and good environmental benignity.[21-22] However, the disadvantages of $ZnCo_2O_4$ and NiO are also obvious. In particular, simple nanostructure, poor intrinsic conductivity and giant volume change of either $ZnCo_2O_4$ or NiO nanostructures during lithium insertion/deinsertion reaction will lead to crack of electrode films in the subsequent electrical isolation and fast capacity fading. All these drawbacks unavoidably constitute a major obstacle for their practical application in LIBs.[23] To overcome the above-mentioned issues, efforts have been extensively afforded to

exploit different novel nanostructures (nanotubes, nanoplates and nanowires/rods, etc.) of $ZnCo_2O_4$[24-26] and NiO,[27-28] respectively. Inspired by combining unique properties of individual constituents as previously demonstrated concerns, we envision fabricating the novel core/shell nanowire arrays, which can exhibit intriguing properties by taking advantage of 3D hierarchical structural features, nanometer-size effects and good stability of the secondary-nanostructure assemblies.[12] Therefore, it is also meaningful to investigate the potential application of 3D ZCO/NiO NWs as binder and additive-free anode materials in LIBs.

Herein, we demonstrate that the freestanding 3D ZCO/NiO NWs were fabricated by a simple, cost-effective hydrothermal growth followed by chemical bath deposition methods, in which the surface of $ZnCo_2O_4$ nanowire cores are enclosed by ultra-thin NiO nanosheet shells (see Fig. 1). Fortunately, it holds several favourable merits as following: (1) both hydrothermal synthesis and chemical bath deposition method have been proved to be an effective, low cost and applicable technique; (2) long ZCO NWs serve as both the backbone and conductive connection for NiO nanosheets, which can obviously increase the robust hierarchical porosity and high surface area of hybrid feature; (3) as a shell, ultrathin nanosheet-like NiO enlarges the interface area with electrolyte and protects the inner $ZnCo_2O_4$ backbone, which can boost the electrochemical reaction and improve the durability; (4) ZCO/NiO NWs grown on Ni foam as LIBs anode may not need any ancillary additives such as carbon black and polymer binder. Due to the unique advantages of freestanding core/shell nanowire arrays, the resulting hierarchical ZCO/NiO NWs exhibit higher capacity, enhanced rate capability and improved cycling stability compared to pristine ZCO NWs when applied as the binder and additive-free anode materials for LIBs.

## Experimental

### Materials Preparation

#### Synthesis of ZCO NWs on 3D Ni foam

In a typical process,[21] 0.2 mmol zinc nitrate ($Zn(NO_3)_2{\cdot}6H_2O$), 0.4 mmol cobalt nitrate ($Co(NO_3)_2{\cdot}6H_2O$), 0.4 mmol ammonium fluoride ($NH_4F$), and 1 mmol urea ($CO(NH_2)_2$) were added to a given amount (25 ml) of distilled water, the resulting homogeneous solution was transferred into a Teflon-lined stainless autoclave. After putting a piece of cleaned Ni foam substrate (2 cm×4 cm), the autoclave was sealed and maintained at 120 °C for 5 h, then cooling down to room temperature. The samples were washed with deionized water for several times and dried at 60 °C for 12 h in vacuum oven. Finally, the ZCO NWs samples with black colour were thermal treated at 400 °C for 2 h in a tube furnace.

#### Synthesis of ZCO/NiO NWs on 3D Ni foam

The as-prepared ZCO NWs samples were used as the scaffold for NiO nanosheets growth by a facile chemical bath deposition (CBD). In a typical process,[29] solution for CBD was prepared by adding 2 mL of aqueous ammonia (25%) to the mixture of 10 mL of 1 M nickel sulfate and 8 mL of 0.25 M potassium persulfate in a 50 mL Pyrex beaker. Then ZCO NWs were used as the growth substrate and placed vertically in the Pyrex beaker, which was shaken by a KS 130 Shakers (IKA) with the speed of 250 rpm. After immersing into the CBD solution for 1 h at room temperature, the substrate was taken off and rinsed with a lot of distilled water and ethanol for several times, respectively. This substrate was then dried at 60 °C for 12 h in vacuum oven. Finally, the substrate was annealed at 300 °C for 1 h in a tube furnace to obtain the final product (brown colour).

### Materials Characterization

Powder X-ray diffraction (XRD) patterns were collected using an X-ray diffractometer with Cu Kα radiation (λ=1.5418Å). Scanning electron microscopy (SEM) images were obtained using a HITACHI S-4300 microscope. High-resolution transmission electron microscopy (HRTEM) observation and energy-dispersive X-ray spectroscopy (EDS) elemental mapping were carried out on a HRTEM JEM-2010FEF instrument. Nitrogen sorption analysis was performed on a Micromeritics (NOVA 4200e) analyzer at 77 K. The Brunauer–Emmett–Teller (BET) surface area was calculated from the linear part of the BET plot. The pore size distribution was derived from the adsorption branch of the isotherm. Raman spectroscopy was performed using a WITEC CRM200 Raman system equipped with a 532 nm laser source and a 100× objective lens.

### Electrochemical Measurement

Ni foam with samples covered was cut into round pieces (diameter ≈ 13 mm). A piece of the samples was used directly at the working electrode without any polymeric binder or carbon black. The CR2016 Coin-type cells were assembled in an Ar-filled glovebox (Mbraun, Unilab, Germany) by directly using the ZCO-NiO (loading density ≈ 0.43mg $cm^{-2}$) and ZCO (loading density ≈ 0.28 mg $cm^{-2}$) on Ni foam as the anode materials, with a Li-metal circular foil (0.59 mm thick) as the counter and reference electrode, a microporous polypropylene membrane as the separator, and 1.0 M solution of $LiPF_6$ in mixed ethylene carbonate (EC) and diethyl carbonate (DEC) (EC : DEC, 1 : 1 by volume) as the electrolyte. The cell was aged for 15 h before measurement. Cyclic voltammetry (CV, 0.01−3.0 V, 0.5 mV $s^{-1}$) was carried out on an electrochemical workstation (CHI 760D). Galvanostatic charging/discharging tests were performed on a NEWARE battery tester at different current rates with a voltage window of 0.01−3.0 V (vs. $Li^+$/Li). The electrochemical impedance spectroscopy (EIS) measurement was performed with the open circle potential by applying an AC voltage of 5 mV over the frequency range from 100 kHz to 0.1 Hz.

## Results and Discussion

Our strategy for the fabrication of freestanding 3D ZCO/NiO NWs on the 3D Ni foam substrate followed the two-step process is schematically depicted in Fig. 1. Firstly, self-assembled ZCO NWs were directly grown on the 3D Ni foam substrate. The obtained ZCO NWs are uniformly aligned onto the Ni foam surfaces without secondary nanostructures (Fig. 2a and b). Close observation on the nanowires displays that individual ZCO nanowire with the average diameter of 100 nm is porous (Fig. 2b, inset), which is obviously different from the precursor

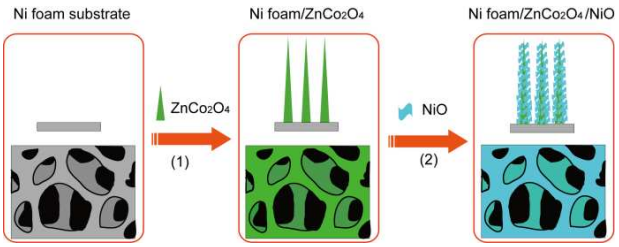


**Fig. 1** Schematic illustration of fabrication processes of ZCO/NiO NWs directly on the Ni foam substrate.

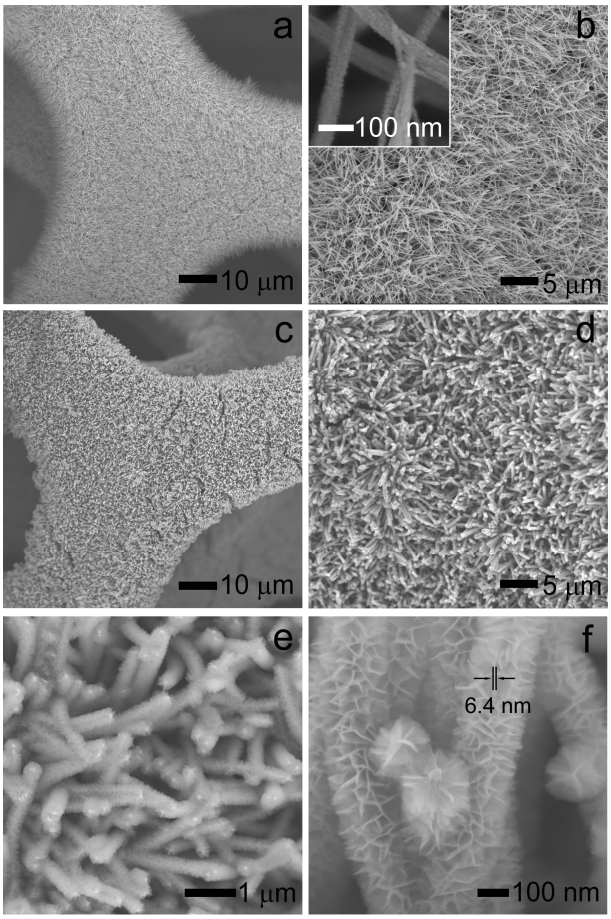


**Fig. 2** SEM images of (a, b) ZCO NWs and (c-f) ZCO/NiO NWs grown on the 3D Ni foam substrate.

ZCO NWs because of the annealing treatment reason (Fig. S1). After applying the controllable deposition of NiO nanosheets on the surface of ZCO NWs by CBD, the nanostructures of core/shell NWs are formed. An overview images (Fig. 2c-d) illustrate the as-prepared ZCO/NiO NWs are still distributed uniformly and adhered firmly onto the Ni foam surface but a fuzzy surface, and the average length of NWs is about 7.0 μm (Fig. S2). Further close observation shows the surfaces of ZCO nanowire backbones are covered by the high densities of the secondary NiO nanosheets (Fig. 2e-f). These NiO nanosheets are highly connected with each other to form the network structures (Fig. 2e). Also, the diameter of individual core/shell ZCO/NiO nanowire is approximately 200 nm, and the average thickness of

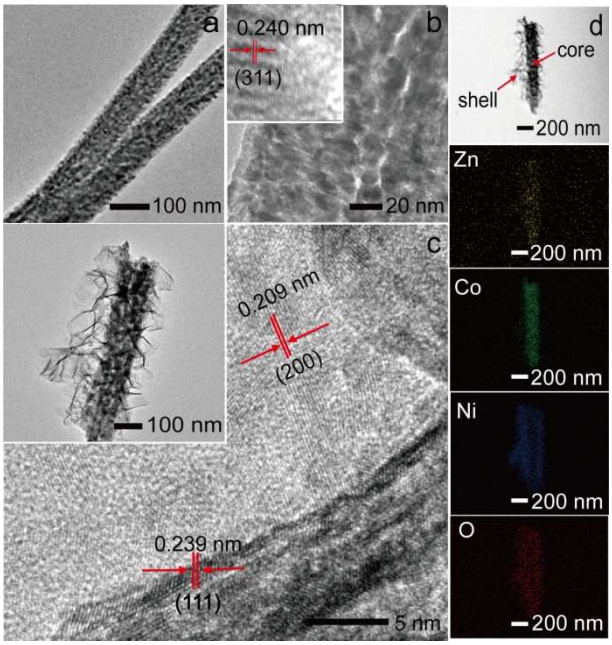


**Fig. 3** TEM images of (a, b) ZCO nanowire (Lattice resolved HRTEM image inset) and (c) TEM image (inset) and lattice resolved HRTEM image of ZCO/NiO nanowire. (d) TEM image of a single ZCO/NiO nanowire and the corresponding TEM-EDS elemental mapping of Zn, Co, Ni, and O.

the secondary NiO nanosheets is about 6.4 nm (Fig. 2f). The growth mechanism of the core/shell nanowire heterostructures are the "oriented attachment" and "self-assembly" processes (also shown schematically in Fig. 1), which involves a spontaneous self-organization between neighboring particles to share a common crystallographic orientation, followed by joining of these particles at a planar interface. The process is particularly relevant in the nanocrystalline regime, where bonding between the particles reduces overall energy by removing surface energy associated with unsatisfied bonds.[3,13] In our experiments, the ZCO NWs acts as the backbone to guide the NiO preferential deposition. In order to gain more insight into the evolution process of hierarchical ZCO/NiO NWs, a series of time-dependent CBD processes for NiO growth is conduced. It can be seen from the SEM images (Fig. S3) that the ZCO/NiO NWs with different morphologies and nanostructures can be achieved in different stages of deposition times.

Detailed microstructures and compositions of ZCO NWs and ZCO/NiO NWs were further investigated by the TEM. It can be clearly observed that the ZCO nanowire is quite porous, with an average diameter of around 100 nm (Fig. 3a and b), which is composed of numerous nanoparticles of 8–21 nm in size and the interplanar spacing of the (311) plane of the $ZnCo_2O_4$,[21,26] as shown in HRTEM image (Fig. 3b, inset). Compared with the pristine ZCO NWs, a portion of the hierarchical nanostructure of ZCO/NiO NWs presents that highly dense NiO nanosheets are emanated from the surface of an individual ZCO nanowire (Fig. 3c, inset). Evidently, it can be clearly seen that the secondary NiO nanosheets with many pores grow on the surface of the porous ZCO nanowire backbone. It is indicated that ZCO/NiO NWs may exhibit high reaction surface area, which will favour the electron

transportation among the whole core/shell NWs area. Moreover, the HRTEM image (Fig. 3c) taken near the connection reveals that the lattice fringes with spacing of 0.209 nm and 0.239 nm are recognized, which corresponds to the (200) and (111) planar space of cubic NiO, respectively.[22] Additionally, the EDS mapping analysis of a single ZCO/NiO nanowire also confirm the ZCO core/NiO shell hierarchical nanostructure, in which the Zn, Co, Ni and O signals appear the similar shape as shown in corresponding TEM image (Fig. 3d, and Fig. S4). It is indicated that an intriguing core/shell NWs nanostructure has been successfully fabricated. This conclusion can also be supported by the below-mentioned Raman and XRD results. The existence of the NiO and ZCO in the as-prepared ZCO/NiO NWs is reflected in the Raman spectra (Fig. S5).[30-31] Subsequently, the crystal phase of the ZCO NWs and ZCO/NiO NWs were further analyzed by XRD measurement (Fig. S6). All the diffraction peaks in XRD pattern of ZCO NWs can be indexed to spinel $ZnCo_2O_4$ phase (JCPDS Card No. 23-1390).[21] Besides, two peaks located at 43.2° and 62.5° match well with the (200) and (220) planes of cubic NiO[29] (JCPDS Card No. 4-0835) as evidenced from the XRD pattern of ZCO/NiO NWs. These results totally confirm that the adopted synthesis strategy successfully achieves ZCO/NiO NWs nanostructure integrating the ZCO nanowires and NiO nanosheets. In addition, the porosity and specific surface area of ZCO NWs and ZCO/NiO NWs were further investigated, as shown in Fig. S7. It is apparently shown that the pore size distribution of ZCO NWs is within 5–20 nm, while the pore size distribution of ZCO/NiO NWs is around 2–5 nm after the bare ZCO NWs were coated with the NiO nanosheets. Furthermore, ZCO/NiO NWs also exhibit a high specific surface area of 119.9 $m^2\ g^{-1}$, which is almost 1.4 times larger than that of ZCO NWs (85.1 $m^2\ g^{-1}$). Thus it is indicated that ZCO/NiO NWs possess high hierarchical porosity possibly due to that numerous ultrathin NiO nanosheets with porous nanostructure coated on the surface of porous ZCO NWs.

To investigate the electrochemical performance of ZCO NWs and ZCO/NiO NWs, the as-obtained arrays were directly used as anodes for battery assembly without adding any binders or conductive additives. Fig.4a shows the first three CV curves of ZCO/NiO NWs electrode at a scan rate of 0.5 mV $s^{-1}$. In the first cathodic sweep, both ZCO/NiO NWs and ZCO NWs (Fig.S8a) exhibit a clear irreversible reduction peak at about 0.5 V, which is attributed to the formation of solid electrolyte interface (SEI) layer that caused by reduction of the electrolyte, and also the irreversible reduction of $ZnCo_2O_4$ and NiO.[23-24,26,32] However, this reduction peak of ZCO NWs (Fig.S8a) shifts to a higher potential at 0.86 V in the subsequent discharge cycles, suggesting at a different lithium insertion reaction which is in agreement with the previous reports.[21,32] While this reduction peak in ZCO/NiO NWs is replaced by two new peaks at 0.86 and 1.25 V after the first cycle. Comparing with the CV curves of ZCO NWs, the extra peak at 1.25 V can be ascribed to the decomposition of NiO. The significant difference of the CV curves between the 1st and subsequent cycles for ZCO/NiO NWs indicates that it experiences an irreversible transition after the initial discharge process.[21] Meanwhile, in the anodic sweep, the two broad oxidation peaks that located at 1.81 and 2.24 V, corresponding to the oxidation of Zn to $Zn^{2+}$, Co to $Co^{3+}$, and Ni to $Ni^{2+}$.[22-23] The above electrochemical processes of the as-obtained arrays are summarized as following: [22, 27-28]

$$8Li^+ + ZnCo_2O_4 + 8e^- \Leftrightarrow 2Co + Zn + 4Li_2O \quad (1)$$

$$xLi^+ + Zn + xe^- \Leftrightarrow Li_xZn \ (x\leq 1) \quad (2)$$

$$Zn + Li_2O \Leftrightarrow ZnO + 2Li^+ + 2e^- \quad (3)$$

$$Co + Li_2O \Leftrightarrow CoO + 2Li^+ + 2e^- \quad (4)$$

$$3CoO + Li_2O \Leftrightarrow Co_3O_4 + 2Li^+ + 2e^- \quad (5)$$

$$NiO + 2Li^+ + 2e^- \Leftrightarrow Ni^0 + Li_2O \quad (6)$$

$$Ni^0 + Li_2O \Leftrightarrow NiO + 2Li^+ + 2e^- \quad (7)$$

The first cycle discharge ($Li^+$ insertion) and charge ($Li^+$ extraction) profiles of ZCO/ NiO NWs and ZCO NWs are illustrated in Fig. 4b. There is a wide, steady discharging plateau at ~1.0 V in the first cycle, followed by a gradual voltage decrease. Notably, the ZCO/NiO NWs exhibit an initial discharge capacity of 1116.4 mAh $g^{-1}$, which is higher than that of ZCO NWs (919.2 mAh $g^{-1}$). Furthermore, ZCO/NiO NWs also have the lower initial irreversible capacity loss of 30.5%, compared to 34.1% for ZCO NWs, which can be possibly owned to the synergetic effect between $ZnCo_2O_4$ and NiO as well as its unique hierarchical architecture. Additionally, the irreversible capacity loss could be due to the solid electrolyte interphase (SEI) formation and the reduction of metal oxide to metal with $Li_2O$ formation, which is commonly observed for a variety of electrode materials.[23] To gain further insight into the advantage of ZCO/NiO NWs for lithium storage, the rate and cycling performances of the ZCO NWs and ZCO/NiO NWs are also evaluated. Fig. 4c shows the rate performance of the arrays. It's noted that despite the severe capacity degradation in the first 10 cycles, ZCO/NiO NWs always deliver two to three times higher specific capacities than that of ZCO NWs with the current density increasing from 0.2 A $g^{-1}$ to 0.8 A $g^{-1}$. Moreover, with the current rate being lowered back to 0.1 A $g^{-1}$, both electrodes are able to recover to high capacity again. In addition, EIS measurements of ZCO NWs and ZCO/NiO NWs electrodes are also performed to probe the kinetic properties of the ZCO/NiO NWs, as shown in Fig. S8b. Apparently, the resulting Nyquist plots exhibit two distinct parts, including a semicircle in the high frequency region and a sloped line in the low frequency region. It is noted that the diameter of the semicircle for the ZCO/NiO NWs (44.8 Ω) is obviously smaller than that of the ZCO NWs (62.8 Ω), while the contact resistances between electrode materials and electrolyte are similar, which hint that ZCO/NiO NWs possess low charge-transfer resistances. These results suggest the coated NiO nanosheets shell coated on the ZCO NWs can not only enable much easier charge transfer at the electrode/electrolyte interface compared with the ZCO NWs, but also largely enhance the electronic conductivity of the ZCO/NiO NWs during the cycling processes.[22] As expected, Fig. 4d depicts the cycling performance of ZCO/NiO NWs electrode up to 50 cycles as well as ZCO NWs electrode. It demonstrates a large drop in capacity of second cycle for two electrodes due to the initial irreversible loss. Despite the relatively faster capacity fading behaviour, ZCO/NiO NWs manifest much larger capacity and significant improved cycling stability comparing to the pristine ZCO NWs. For example, the capacities of the 50th cycle are found to be 357 mA h $g^{-1}$ and 152 mA h $g^{-1}$ for ZCO/NiO NWs electrode and ZCO NWs electrode, respectively. These above results provide effective evidence about the enhancement of the composite materials over single

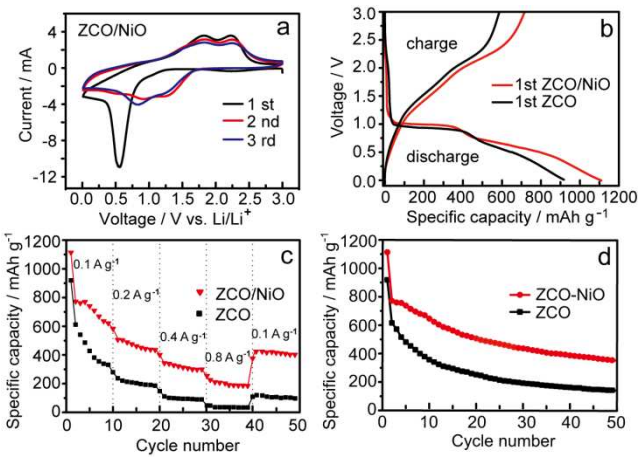


**Fig. 4** (a) The first three CV curves of ZCO/NiO NWs at a scanning rate of 0.5 mV $s^{-1}$. (b) The first discharge/charge profiles of ZCO NWs and ZCO/NiO NWs at a current density of 0.1 A $g^{-1}$. (c) Rate capability of ZCO NWs and ZCO/NiO NWs at different current densities. (d) Cycling performance of ZCO NWs and ZCO/NiO NWs at a constant current density of 0.1 A $g^{-1}$.

ones, while the enhancement is not simply a result of the introduction of a higher capacity component.[3,10] Instead, it more likely originates from the unique nanostructure of the composite electrode. The improved performance of ZCO/NiO NWs can be attributed to the unique hierarchical nanostructures of the ZCO/NiO NWs, which is elaborated as follows.[10-11,33-35] (1) the hierarchical ZCO/NiO NWs possess larger surface area and thus have an enhanced portion of exposed surfaces, which provides more active sites for Li ions accesses to ensure a high utilization of electrode materials;[23,36-38] (2) the novel 3D array architecture with porous texture can provide the facile diffusion of electrolyte/ions and thus shortens the transport pathway of Li ions to the surface of the active material, resulting in enhanced rate capability with respect to the pristine ZCO NWs.[16,36,39] Specially, in comparison with the pristine ZCO NWs, the highly dense NiO nanosheet coated on the ZCO NWs may relieve the stress exerted on inner nanowires caused by severe volume change arising from alloying/dealloying, and thus suppress the degradation of the core ZCO material;[40-41] (3) compared to the ZCO NWs, the porous nature of ZCO/NiO NWs between the interior of ZCO nanowire cores and exterior of NiO nanosheet is beneficial to relieve the strain induced by the volume change during cycling, therefore leading to the improved cycling stability;[42-44] (4) the increased electronic conductivity may also be an important factor in improving the electrochemical performance of the electrode materials.[45-48] The higher capacity, improved rate capability and cycling stability of ZCO/NiO NWs composite electrode indicate the efficiency of our protocol in constructing 3D core/shell nanostructure to improve the electrochemical performance of the electrode materials.

## Conclusions

In conclusion, we have demonstrated the facile and controllable synthesis of freestanding hierarchical ZCO/NiO NWs on Ni foam by applying a simple and cost-effective hydrothermal growth combined with a subsequent chemical bath deposition method. High-resolution scanning and transmission electron microscopies reveals that the ultra-thin NiO nanosheets are uniformly grew on the porous $ZnCo_2O_4$ nanowire with many interpartical mesopores, resulting in the formation of 3D core/shell nanowire arrays with hierarchical architecture. The as-prepared arrays were directly used as the binder and additive-free anodes for LIBs by using a standard half cell configuration. The results show that the ZCO/NiO NWs have a higher capacity, improved rate capability and cycling stability with respect to the pristine ZCO NWs, which is mainly attributed to the synergistic contribution between ZCO nanowire cores and NiO nanosheet shells, as well as the high surface area and porous array geometry. It is expected that present synthetic protocol can be further extended to build up other 3D core/shell nanostructures based on low-cost and earth abundant materials for energy storage applications.

## Acknowledgements

This work is supported by the Singapore National Research Foundation under NRF RF Award no. NRF-RF2010-07, A*Star SERC PSF grant 1321202101 and MOE Tier 2 MOE2012-T2-2-049.

## Notes and references

[a]*Division of Physics and Applied Physics, School of Physical and Mathematical Sciences, Nanyang Technological University, 637371, Singapore. E-mail: yuting@ntu.edu.sg*
[b]*Xinjiang Uygur Autonomous Region Product Quality Supervison and Inspection Institute, 830011, China.*
[c]*School of Materials Science and Engineering, Nanyang Technological University, 63639798, Singapore.*
[d]*Department of Physics, Faculty of Science, National University of Singapore, 117542, Singapore.*
[e]*Graphene Research Centre, National University of Singapore, 117546, Singapore.*
† Electronic Supplementary Information (ESI) available: [details of any supplementary information available should be included here]. See DOI: 10.1039/b000000x/

1 C. Q. Shang, S. M. Dong, S. Wang, D. D. Xiao, P. X. Han, X.G. Wang, L. Gu and G. L. Cui, *ACS Nano*, 2013, **7**, 5430-5436.
2 S. Han, C. Li, Z. Q. Liu, B. Lei, D. H. Zhang, W. Jin, X. L. Liu, T. Tang and C. W. Zhou, *Nano Lett.*, 2004, **4**, 1241-1246.
3 L. Q. Mai, F. Yang, Y. L. Zhao, Q. X. Xu, L. Xu and Y. Z. Luo, *Nat. Commun.*, 2011, **2**, 381.
4 A. S. Aricò, P. Bruce, B. Scrosati, J. M. Tarascon and W. Van Schalkwijk, *Nat. Mater.*, 2005, **4**, 366-377.
5 K. Wang, J. Chen, W. Zhou, Y. Zhang, Y. Yan, J. Pern and A. Mascarenhas, *Adv. Mater.*, 2008, **20**, 3248-3253.
6 W. Li, J. P. Yang, Z. X. Wu, J. X. Wang, B. Li, S. S. Feng, Y. H. Deng, F. Zhang and D. Y. Zhao, *J. Am. Chem. Soc.*, 2012, **134**, 11864-11867.
7 S. M. Dong, X. Chen, L. Gu, X. H. Zhou, L. F. Li, Z. H. Liu, P. X. Han, H. X. Xu, J. H. Yao, H. B. Wang, X. Y. Zhang, C. Q. Shang, G. L. Cui and L. Q. Chen, *Energy Environ. Sci.*, 2013, **4**, 3502-5408
8 Y. Wu, J. Xiang, C. Yang, W. Lu and C. M. Lieber, *Nature*, 2004, **430**, 61-65.
9 C. W. Cheng, B. Liu, H. Y. Yang, W. W. Zhou, L. Sun, R. Chen, S. F. Yu, J. X. Zhang, H. Gong, H. D. Sun and H. J. Fan, *ACS Nano*, 2009, **3**, 3069-3076.
10 W. W. Zhou, Y. Y. Tay, X. T. Jia, D. Y. Yau Wai, J. Jiang, H. H. Hoon and T. Yu, *Nanoscale*, 2012, **4**, 4459-4463.

11 Y. S. Luo, J. S. Luo, J. Jiang, W. W. Zhou, H. P. Yang, X. Y. Qi, H. Zhang, H. J. Fan, D. Y. W. Yu, C. M. Li and T. Yu, *Energy Environ. Sci.*, 2012, **5**, 6559-6566.

12 W. Q. Zeng, F. P. Zheng, R. Z. Li, Y. Zhan, Y. Y. Li and J. P. Liu, *Nanoscale*, 2012, **4**, 2760-2765.

13 X. H. Xia, J. P. Tu, Y. Q. Zhang, X. L. Wang, C. D. Gu, X. B. Zhao and H. J. Fan, *ACS Nano*, 2012, **6**, 5531-5538.

14 G. R. Li, Z. L. Wang, F. L. Zheng, Y. N. Ou and Y. X. Tong, *J. Mater. Chem.*, 2011, **21**, 4217-4221.

15 X. H. Lu, T. Zhai, X. H. Zhang, Y. Q. Shen, L. Y. Yuan, B. Hu, L. Gong, J. Chen, J. Zhou, Y. X. Tong and Z. L. Wang, *Adv. Mater.*, 2012, **24**, 938-944.

16 J. Yan, A. Sumboja, E. Khoo and P. S. Lee, *Adv. Mater.*, 2011, **23**, 746-750.

17 H. Wang, D. Ma, X. Huang, Y. Huang and X. Zhang, *Sci. Rep.*, 2012, **2**, 701.

18 J. P. Liu, J. Jiang, C. W. Cheng, H. X. Li, J. X. Zhang, H. Gong and H. J. Fan, *Adv. Mater.*, 2011, **23**, 2076-2081.

19 L. Yu, G. Q. Zhang, C. Z. Yuan and X. W. Lou, *Chem. Commun.*, 2013, **49**, 137-139.

20 J. Jiang, Y. Y. Li, J. P. Liu, X. T. Huang, C. Z. Yuan and X. W. Lou, *Adv. Mater.*, 2012, **24**, 5166-5180.

21 B. Liu, J. Zhang, X. F. Wang, G. Chen, D. Chen, C. W. Zhou and G. Z. Shen, *Nano Lett.*, 2012, **12**, 3005-3011.

22 B. Varghese, M. V. Reddy, Z. Yanwu, C. S. Lit, T. C. Hoong, G. V. S. Rao, B. V. R. Chowdari, A. T. Shen Wee, C. T. Lim and C. H. Sow, *Chem. Mater.*, 2008, **20**, 3360-3367.

23 Y. Sharma, N. Sharma, G. V. Subba Rao and B. V. R. Chowdari, *Adv. Funct. Mater.*, 2007, **17**, 2855-2861.

24 W. Luo, X. L. Hu, Y. M. Sun and Y. H. Huang, *J. Mater. Chem.*, 2012, **22**, 8916-8921.

25 Y. C. Qiu, S. H. Yang, H. Deng, L. M. Jin and W. S. Li, *J. Mater. Chem.*, 2010, **20**, 4439-4444.

26 N. Du, Y. F. Xu, H. Zhang, J. X. Yu, C. X. Zhai and D. R. Yang, *Inorg. Chem.*, 2011, **50**, 3320-3324.

27 S. A. Needham, G. X. Wang and H. K. Liu, *J. Power Sources*, 2006, **159**, 254-257.

28 D. Su, M. Ford and G. Wang, *Sci. Rep.*, 2012, **2,** 924.

29 X. H. Xia, J. P. Tu, J. Zhang, X. L. Wang, W. K. Zhang and H. Huang, *Sol. Energy Mater. Sol. Cells*, 2008, **92**, 628-633.

30 N. Mironova-Ulmane, A. Kuzmin, I. Steins, J. Grabis, I. Sildos and M. Pars, *J. Phys. Conference Series.*, 2007, **93**, 012039.

31 K. Samanta, P. Bhattacharya, R. S. Katiyar, W. Iwamoto, P. G. Pagliuso and C. Rettori, *Phys. Rev. B: Condens. Matter.*, 2006, **73**, 245213.

32 C. C. Ai, M. C. Yin, C. W. Wang and J. T. Sun, *J. Mater. Sci.*, 2004, **39**, 1077-1079.

33 G. F. Ortiz, I. Hanzu, P. Lavela, P. Knauth, J. L. Tirado and T. Djenizian, *Chem. Mater.*, 2010, **22**, 1926-1932.

34 S. L. Xiong, J. S. Chen, X. W. Lou and H. C. Zeng, *Adv. Funct. Mater.*, 2012, **22**, 861-871.

35 W. W. Zhou, J. Zhu, C. W. Cheng, J. P. Liu, H. P. Yang, C. X. Cong, C. Guan, X. T. Jia, H. J. Fan, Q. Y. Yan, C. M. Li and T. Yu, *Energy Environ. Sci.*, 2011, **4**, 4954-4961.

36 P. L. Taberna, S. Mitra, P. Poizot, P. Simon and J. M. Tarascon, *Nat. Mater.*, 2006, **5**, 567-573.

37 Y. Liu, C. H. Mi, L. H. Su and X. G. Zhang, *Electrochim. Acta*, 2008, **53**, 2507-2513.

38 W. W. Zhou, C. W. Cheng, J. P. Liu, Y. Y. Tay, J. Jiang, X. T. Jia, J. Zhang, H. Gong, H. H. Hng, T. Yu and H. J. Fan, *Adv. Funct. Mater.*, 2011, **21**, 2439-2445.

39 Y. N. NuLi, P. Zhang, Z. P. Guo, H. K. Liu and J. Yang, *Electrochem. Solid State Lett.*, 2008, **11**, A64-A67.

40 X. J. Zhu, Y. W. Zhu, S. Murali, M. D. Stoller and R. S. Ruoff, *ACS Nano*, 2011, **5**, 3333-3338.

41 Y. G. Li, B. Tan and Y. Y. Wu, *Nano Lett.*, 2008, **8**, 265-270.

42 Y. Wang, H. C. Zeng and J. Y. Lee, *Adv. Mater.*, 2006, **18**, 645-649.

43 Y. Wang, H. Xia, L. Lu and J. Y. Lin, *ACS Nano*, 2010, **4**, 1425-1432.

44 Y. Wang and G. Z. Cao, *Adv. Mater.*, 2008, **20**, 2251-2269.

45 W. Ai, L. H. Xie, Z. Z. Du, Z. Y. Zeng, J. Q. Liu, H. Zhang, Y. H. Huang, W. Huang and T. Yu, *Sci. Rep.*, 2013, **3**, 2341.

46 J. S. Chen, C. M. Li, W. W. Zhou, Q. Y. Yan, L. A. Archer and X. W. Lou, *Nanoscale*, 2009, **1**, 280-285.

47 J. F. Li, J. Z. Wang, D. Wexler, D. Q. Shi, J. W. Liang, H. K. Liu, S. L. Xiong and Y. T. Qian, *J. Mater. Chem. A*, 2013, **1**, 15292-15299

48 L. Li, Y. W. Yang, G. H. Li and L. D. Zhang, *Small*, 2006, 2, 548-553.